JCTC Journal of Chemical Theory and Computation

Article

pubs.acs.org/JCTC

Chemiluminescence of Coelenterazine and Fluorescence of Coelenteramide: A Systematic Theoretical Study

Shu-Feng Chen,[†] Isabelle Navizet,[‡,§] Daniel Roca-Sanjuán,[∥] Roland Lindh,[∥] Ya-Jun Liu,*[,†] and Nicolas Ferré*[,⊥]

[†]Key Laboratory of Theoretical and Computational Photochemistry (Beijing Normal University), Ministry of Education, College of Chemistry, Beijing Normal University, Beijing 100875, China

[‡]Université Paris-Est, Laboratoire Modélisation et Simulation Multi Echelle, MSME UMR 8208 CNRS, 5 bd Descartes, 77454 Marne-la-Vallée, France

[§]Molecular Science Institute, School of Chemistry, University of the Witwatersrand, PO Wits Johannesburg 2050, South Africa

[∥]Department of Chemistry—Ångström, the Theoretical Chemistry Programme, Uppsala University, P.O. Box 518, S-75120 Uppsala, Sweden

[⊥]Aix-Marseille Université, Institut de Chimie Radicalaire, 13397 Marseille Cedex 20, France

Supporting Information

ABSTRACT: A systematic investigation of the structural and spectroscopic properties of coelenteramide has been performed at the TD-CAM-B3LYP/6-31+G(d,p) level of theory, including various fluorescence and chemiluminescence states. The influence of geometric conformations, solvent polarity, protonation state, and the covalent character of the O−H bond of the hydroxyphenyl moiety were carefully studied. Striking differences in geometries and electronic structures among the states responsible for light emission were characterized. All fluorescence states can be described as a limited charge transfer process for a planar amide moiety. However, the chemiluminescence state is characterized by a much larger charge transfer that takes place over a longer distance. Moreover, the chemiluminescent coelenteramide structure exhibits an amide moiety that is no longer planar, in agreement with recent, more accurate *ab initio* results [Roca-Sanjuán et al. *J. Chem. Theory Comput.* **2011**, *7*, 4060]. Because the chemiluminescence state appears to be completely dark, a new mechanism is tentatively introduced for this process.

INTRODUCTION

The chemiluminescent compound coelenterazine is related to the bioluminescence reactions of a wide range of marine organisms such as coelenterates, fish, squid, and shrimp.[1−6] The bioluminescence reaction involves an oxidative decarboxylation of the coelenterazine, resulting in the excited state (S_1) of the product coelenteramide **2** (Figure 1).[7,8] When the electronically excited **2** relaxes to its ground state (S_0), it produces a blue light with a spectrum maximum in the range 465−495 nm, depending on the type of organism.[9] The reaction mechanism is thought to involve the breakdown of the dioxetanone intermediate **1** (Figure 1) and formation of a carbonyl group, which is common for all coelenterazine-dependent photoproteins and luciferin−luciferase systems.[10] Using a model study of the chemiluminescence of a coelenterazine analogue in an aprotic solvent, McCapra et al. concluded that the amide anion is the emitter in aequorin bioluminescence.[5] However, it is thought that the amide anion, being a very strong base, is protonated immediately in any protic environment.[6] Hirano et al. conducted a systematic study of the fluorescence of a **2** analog and concluded that the phenolate anion $\mathbf{2O}^-$, rather than the amide anion, is the blue-light emitter in aequorin bioluminescence.[11−14] Thus, $\mathbf{2O}^-$ is generally accepted as the light emitter in photoprotein bioluminescence.[9,15,16] On the other hand, experimental mutant or semisynthetic studies of aequorin and obelin showed two-peak emission spectra.[17−21] The lower energy peak is assigned to emission from the excited $\mathbf{2O}^-$, and the higher energy peak is assigned to excited **2H**. Based on structural studies of Ca^{2+}-discharged obelin and dynamic studies of excited-state **2** bound to Ca^{2+}-discharged obelin and aequorin, **2H** was suggested as the primary excited state product.[16,19]

Experimental research into the chemiluminescence of coelenterazine analogues and the fluorescence of **2** derivatives has been reported. Wu et al. studied the chemi- and bioluminescence of coelenterazine analogues and determined the fluorescence spectra of the reaction products.[22] The chemiluminescence emission maximum appears to be the same as the bioluminescence emission maximum, while the product fluorescence emission maximum is approximately 50 nm different from that of bioluminescence. The fluorescence properties of **2** and its analogues have been extensively studied in various organic solvents, and five possible emitters have been proposed.[23] Hirano and co-workers investigated analogues of **2** in various base/solvent combinations, concluding that the fluorescence properties of **2** depend on structural modifications induced by the putative formation of an ion pair between the coelenteramide analogue and base molecules, as well as on the solvent polarity.[11,12]

All of these experimental data give rise to the following questions: What are the electronic and geometric structures of

Received: May 7, 2012
Published: July 10, 2012

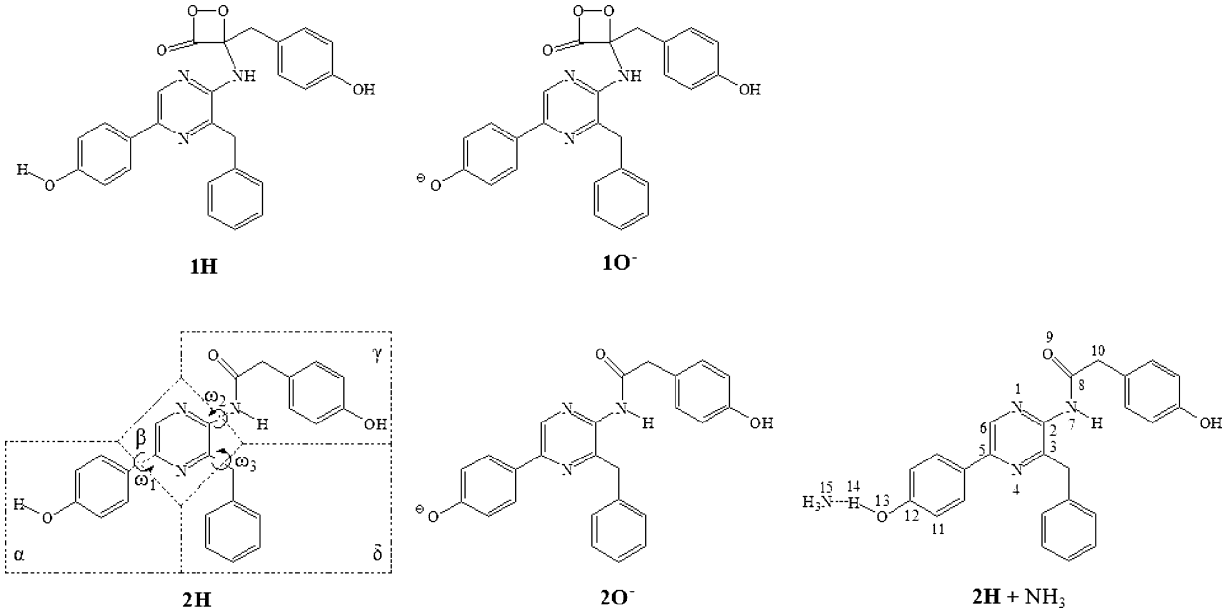

Figure 1. Molecular structures and atomic labels for peroxidized coelenterazine (**1**, protonated **1H** or not protonated **1O**$^-$), coelenteramide (**2**, protonated **2H** and not protonated **2O**$^-$), and **2H** + NH_3 complex.

the chemi- and bioluminescent species? Do they differ from those of the fluorescent species? How do the surroundings modify the light emission properties of the molecule? These questions deserve theoretical investigation.

Isobe et al. theoretically investigated the thermal decomposition of the peroxidized coelenterazine **1**.[24] Their analysis demonstrated the importance of surrounding effects in terms of local basicity and hydrogen bonding. Based on PM3 computations, Tomilin et al. concluded that the bioluminescence spectrum of obelin was determined by the position of the proton between the oxygen atom of the phenolic group of **2** (α moiety, see Figure 1) and the nitrogen atom of His22.[25] Due to the complexity of molecule **2**, no state-of-the-art multireference *ab initio* study on its spectral properties has been published. Nevertheless, we recently used a model coelenteramide compound, 2-acetamido-3-methylpyrazine, whose luminescent and fluorescent structures, we demonstrated, differ dramatically.[26] In the present work, we theoretically study the chemiluminescence of coelenterazine and the fluorescence of **2H** and **2O**$^-$ using the time-dependent density functional (TD-DFT) method[27−30] with the CAM-B3LYP[31,32] functional. The conformational space of **2** is systematically explored, and both the fluorescent and chemiluminescent states are considered, as in ref 26. Finally, the environmental effects are qualitatively taken into account using implicit solvent models and ion-pair structures.

■ COMPUTATIONAL DETAILS

All calculations were performed at the TD-DFT level of theory using the CAM-B3LYP functional (because the chemi- and bioluminescence mechanisms involve charge-transfer excited states)[33−35] and the 6-31+G(d,p) basis set. Frequency calculations allowed us to verify the nature of all S_0 stationary points. These calculations were performed in the gas phase and with solvent models for benzene and acetonitrile (ACN). The solvent effect was taken into account by means of the polarizable continuum model (PCM)[36,37] for the nonpolar solvent benzene and the conductor-like polarizable continuum model (CPCM)[38] for the polar solvent ACN. Standard cavity models using UFF radii were used. Charge distributions in **2** were computed by means of Natural Population Analysis (NPA).[39] Atomic charges were summed for all the atoms in a given subgroup (denoted α, β, γ, and δ in Figure 1). The Gaussian 09[40] software was used for all calculations.

Conformations of 2H and 2O$^-$**.** The X-ray crystallographic structure of **2** in Ca^{2+}-discharged obelin (PDB code: 2F8P.pdb) was used as a starting point (conformation **AI**). In this study, we considered only the neutral amide species as the most probable primary excited-state product for both chemiluminescence and bioluminescence.[6,16] Because **2** is a rather large molecular system, it may exist as different conformational isomers related by the relative orientations of the three side groups with respect to the central pyrazine moiety (see Figure 1). Consequently, we performed a conformational investigation by means of simulated annealing[41] at the semiempirical PM6[42] level of theory, after which four and six low-energy conformers of **2H** and **2O**$^-$ were found, respectively. These structures were reoptimized using DFT to obtain one (**BI**) and two (**BI** and **CI**) new conformers for **2H** and **2O**$^-$, respectively.

Based on the hypothesis that a fluorescence maximum intensity corresponds to a minimum energy structure on S_1, close to a computed S_0 conformation, the corresponding S_1 structures were optimized (conformations **AI*** and **BI*** for **2H**; **AI***, **BI***, and **CI*** for **2O**$^-$). To find other possible ground state conformations, these S_1 structures were subsequently reoptimized in S_0, resulting in conformations **AII** and **BII**, for **2H**, and **AII**, **BII**, and **CII**, for **2O**$^-$.

To the best of our knowledge, the excited-state equilibrium structures of the full coelenteramide molecule have not previously been characterized in the vicinity of the region where the system hops to the excited-state surface in the chemiluminescence reaction (i.e., a S_0/S_1 conical intersection). Isobe et al. investigated the thermal decomposition of the peroxidized coelenterazine, which corresponds to ground-state reactivity.[24] Based on previous findings for small molecular models,[10,26,35] the transition state (TS) structure of the

decomposition reaction can be qualitatively predicted in the vicinity of the region of S_0/S_1 near-degeneracy, and therefore, we decided to use the reported TS geometries of models $(O_XH, N_1H, O_YH)^0$ and $(O_X, N_1H, O_YH)^{-1}$ (for the labels, see ref 24) as new starting structures to find other relevant ground- and excited-state conformations. Geometry optimization of the TS (main characteristics given in the Supporting Information) and intrinsic reaction coordinate (IRC) calculations were carried out in the ground state, and after removal of the leaving CO_2 moiety, the new structure was denoted **DI**. Eventually, this conformation was used to find a new S_1 structure **DI*** in the case of **2H** (the corresponding $\mathbf{2O^-}$ calculation did not converge), which was further optimized in S_0 to reach another ground state minimum, **DII**.

The determination of chemiluminescent structures is difficult because, in principle, we need to compute the complete reaction path in S_0 until the transition to S_1 occurs and then follow the reaction in the populated excited state. Although a few recent techniques exist to locate approximate conical intersections at the TD-DFT level of theory,[43−46] the two-state nature of these peculiar structures is problematic for any single-reference method. Hence, we avoid conical intersection computations and focus on the determination of the chemiluminescence state using two different strategies. The first, as mentioned, consists of using the TS as the starting structure for the S_1 geometry optimization after removing CO_2. The second strategy makes use of the ground-state reaction path, selecting the structure characterized by the smallest $S_0 \rightarrow S_1$ transition energy. Note that this last strategy assumes that the thermal decomposition and chemiluminescence reaction coordinates are roughly parallel. In both cases, we obtained the same conformation **DII*** in the case of **2H** (the corresponding $\mathbf{2O^-}$ calculation did not converge). This conformation is identical to **DI***.

Finally, the conformational complexity of coelenteramide prompted us to build our own chemiluminescent model **1** by adding a CO_2 moiety to the **AI** conformation of **2**. We then used the same strategies as in the case of Isobe's structure:[24] TS determination of S_0 followed by IRC resulting in conformation **EI**. Geometry optimization on S_1 led to the minimum-energy structure **EI***, identical to **BI*** in the case of **2H** (unconverged for $\mathbf{2O^-}$). From the same TS structure, a transition to S_1 and geometry optimization led to a new excited state conformation **EII***. Decay to S_0 leads back to **EI** for **2H** and to a new conformation **EII** in the case of $\mathbf{2O^-}$.

Any other attempts (from higher energy PM6 structures or different points on the IRC path) to find other conformations were unsuccessful. The strategies presented above are schematically depicted in Figure 2 for **2H** and $\mathbf{2O^-}$. To summarize, all the excited state conformers are indicated with the symbol **XI*** (**X** = **A**, **B**, **C**, ...) when their structures have been optimized from a starting S_0 minimum energy geometry **XI**. Conversely, the ground state conformation **EII** was obtained using **EII*** as a starting structure.

Effect of the Covalent Character of the Phenolic O···H Bond. The spectroscopic properties of **2** analogues have been experimentally measured using various base/solvent combinations; absorption and fluorescence maxima depend on the selected base/solvent combination.[11−13,23] From a structural viewpoint, the effect of both the acidity of the $\mathbf{2O^-}$ countercation and the polarity of the microenvironment can be qualitatively understood considering the covalent character of the $O_{13}\cdots H_{14}$ bond. Therefore, we used a simple model **2H**

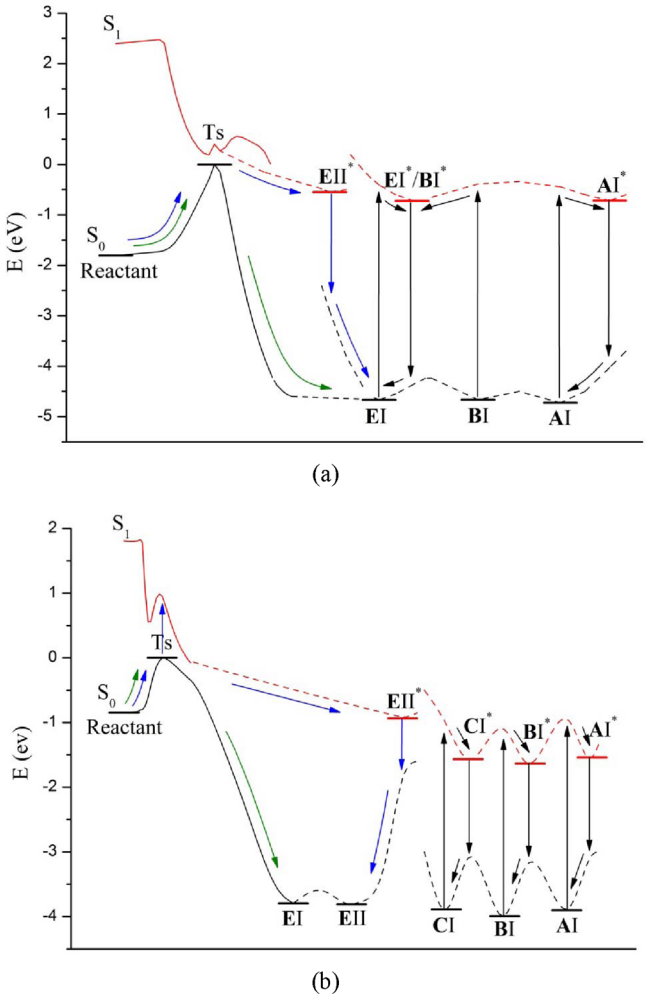

Figure 2. Energy profiles (black, S_0; red, S_1) for (a) neutral **1H** and **2H**, (b) deprotonated $\mathbf{1O^-}$ and $\mathbf{2O^-}$. Plain lines correspond to the computed IRCs on the ground state. Green arrows illustrate the thermal decomposition path of coelenterazine, while the blue arrows illustrate the chemiluminescence path. Black arrows illustrate the possible excitation/fluorescence paths for coelenteramide. For the sake of clarity, only a set of representative structures has been selected.

(conformation **AI**) + NH_3 in benzene (as shown in Figure 1); to control the degree of covalency of the $O_{13}-H_{14}$ bond, we constrained its length and increased it toward the final state $\mathbf{2O^-}$ + NH_4^+. We added other constraints to avoid spurious interactions between the NH_4^+ and $\mathbf{2O^-}$ moieties. Hence, for a given $O_{13}-H_{14}$ distance ranging from 1.0 to 4.0 Å, the $C_{12}-O_{13}-N_{15}$ valence angle and $C_{11}-C_{12}-O_{13}-N_{15}$ dihedral angle were fixed and all other degrees of freedom were relaxed.

Hirano and co-workers found that $\mathbf{2O^-}$ in benzene is characterized by a fluorescence spectrum similar to the bioluminescence spectrum of aequorin; they concluded that the active site of apoaequorin has a polarity similar to benzene.[12,47] Hence, the effect of the covalent character of the $O_{13}-H_{14}$ bond on the chemiluminescence spectrum of **2** was also considered in the present work using the **2H** (conformation **EII***) + NH_3 model in benzene solvent (using PCM).

Table 1. Selected Bond Lengths (Å) and Dihedral Angles (deg)

			gas phase					in benzene					in ACN				
			ω_1	ω_2	ω_3	θ	$R(C_8-O_9)$	ω_1	ω_2	ω_3	θ	$R(C_8-O_9)$	ω_1	ω_2	ω_3	θ	$R(C_8-O_9)$
2H	S_0	**AI**	−21	−120	47	178	1.221	16	−120	45	178	1.223	25	−118	45	177	1.225
		BI	−21	−57	112	−179	1.216	−23	−52	113	179	1.219	−24	−66	102	179	1.228
		DI	−21	−42	−112	−180	1.215	−23	−44	−113	−180	1.219	−25	−48	−109	−179	1.224
		DII	20	−43	−115	−180	1.215	23	−43	−115	−180	1.218	25	−47	−111	−180	1.224
		EI	21	−58	110	−179	1.216	23	−52	111	179	1.219	25	−68	101	179	1.228
	S_1	**AI***	−5	−54	65	179	1.219	2	−141	47	178	1.223	2	−141	46	178	1.225
		BI*	1	−34	99	−179	1.216	1	−31	99	−179	1.219	1	−33	99	179	1.226
		DI*	1	−30	−120	−179	1.216	0	−30	−118	−180	1.219	1	−32	−116	−179	1.225
		EII*	16	−19	118	139	1.286	15	−16	117	139	1.290	16	−16	117	140	1.296
2O$^-$	S_0	**AI**	−3	−120	52	179	1.224	−7	−116	51	179	1.225	13	−89	60	180	1.230
		BI	−2	129	121	−179	1.226	−6	126	120	−178	1.228	−13	122	117	−179	1.230
		CI	−5	−118	52	177	1.224	−9	−115	50	178	1.226	−13	−108	50	178	1.230
		DI	3	−128	−115	179	1.227	4	−126	−115	180	1.227	16	−121	−114	178	1.228
		EI	2	−81	96	179	1.219	−2	−73	102	179	1.223	13	−72	101	179	1.230
		EII	2	−68	109	−179	1.221	2	−66	109	−179	1.223	13	−72	101	179	1.230
	S_1	**AI***	−89	−123	55	177	1.228	−18	−122	53	178	1.226	5	−122	51	178	1.230
		BI*	−89	129	117	−179	1.230	−90	124	116	−178	1.232	−4	129	114	−179	1.233
		CI*	−89	−118	55	177	1.228	−21	−120	53	178	1.228	3	−122	50	178	1.232
		EI*						15	−57	97	−180	1.224	2	−55	100	180	1.231
		EII*	3	−12	−12	138	1.275	1	108	−9	139	1.284	−1	−7	114	141	1.294

dx.doi.org/10.1021/ct300356j | J. Chem. Theory Comput. 2012, 8, 2796−2807

Table 2. Natural Bond Orbital Charge Distributions for Conformations AI and AI*[a]

			gas phase		in benzene		in ACN	
geometry			S_0	S_1	S_0	S_1	S_0	S_1
2H	α	S_0	0.03	0.05	0.04	0.05	0.04	0.06
		S_1	0.19	−0.04	0.27	0.25	0.30	0.25
	β	S_0	0.10	0.11	0.09	0.06	0.09	0.05
		S_1	−0.12	0.13	−0.20	−0.20	−0.22	−0.19
	γ	S_0	−0.16	−0.18	−0.16	−0.14	−0.16	−0.14
		S_1	−0.12	−0.14	−0.11	−0.08	−0.11	−0.09
2O$^-$	α	S_0	−0.73	−0.91	−0.80	−0.81	−0.86	−0.82
		S_1	−0.03	0.08	−0.13	−0.03	−0.26	−0.25
	β	S_0	−0.05	0.08	−0.01	−0.01	0.03	−0.02
		S_1	−0.71	−0.86	−0.65	−0.77	−0.56	−0.58
	γ	S_0	−0.22	−0.20	−0.20	−0.20	−0.20	−0.18
		S_1	−0.24	−0.23	−0.22	−0.21	−0.20	−0.19

[a]The line entitled geometry indicates the electronic state for which the molecular geometry has been optimized.

RESULTS AND DISCUSSION

Structures. Important geometric parameters for **2H** and **2O**$^-$ in the S_0 and S_1 electronic states are reported in Table 1, including the three torsion angles ω_1, ω_2, and ω_3, and measuring the relative orientations of the different moieties (phenol/phenolate, α; *p*-hydroxyphenylacetamide, γ; and toluene, δ) with respect to the central section (pyrazine, β) of **2**, as shown in Figure 1. Additionally, the pyramidalization angle θ at the carbon center and the carbon−oxygen bond length R are used to monitor the hybridization state of the amide moiety in the γ section of the molecule. Finally, the minimum root mean square deviation superimpositions of the conformations for a given electronic state and a given environment are depicted in Figure S2 (Supporting Information).

We begin with **2H**. The consideration of the three torsion angles ω_1, ω_2, and ω_3, is sufficient to demonstrate that all the five S_0 conformations **AI**, **BI**, **DI**, **DII**, and **EI** are distinct (**AII** being identical to **AI** and **BII** being identical to **EI**: these two conformations are not considered further). Note that the α and β sections are always tilted by a ± 20° angle. **BI** and **EI** conformations differ only in their ω_1 value; the same happens for **DI** and **DII**. The θ and R (1.215−1.221 Å) values clearly indicate an sp^2 hybridization of the amide carbon atom. Increasing the polarity of the surroundings (benzene and ACN solvents, compared to the gas phase) only slightly modifies the geometries, including the largest modification concerning ω_1 in **AI**, which is shifted from −21° (gas phase) to 25° (ACN). The transition to S_1 has strong incidence on the conformer geometries; α and β sections are coplanar in the excited state, and ω_2 angle values are largely reduced (e.g., from −120° to −54° for **AI**). The **BI** and **EI** conformations (differing only in ω_1) end as a single excited minimum, **BI***. For all **XI*** conformations, the amide moiety in the γ section remains planar and the C−O bond length is not affected by the $S_0 \rightarrow S_1$ transition. However, the **EII*** conformation obtained from the TS of the thermal decomposition reaction of **1** clearly differs. The α and β sections are twisted by 16° (similar to the S_0 conformations) and β/γ coplanarity is nearly achieved (ω_2 = −19°). The γ amide θ (139°) and R (1.286 Å) values are dramatically different, evidencing an sp^3 hybridization of the carbon atom similar to the TS structure of **1**. The solvent effects only slightly affect the **2H** S_1 geometries, with the most notable exception of ω_2 in **AI*** (−54° to −141°). In **EII***, the C−O bond length R increases by 1 pm, reaching a value of 1.296 Å going from the gas phase to ACN solvent.

In our previous *ab initio* study of a model coelenteramide molecule, the hybridization of the amide carbon atom was used to distinguish between the fluorescent and chemiluminescent excited states.[24,26,33,35] Now, studying the entire molecule **2H** at the CAM-B3LYP level of theory, the same trend can be retrieved and we can make the hypothesis that all **XI*** conformations are related to the fluorescence of **2H**, while the **EII*** conformation is a minimum-energy structure of the chemiluminescence excited state.

We now turn to **2O**$^-$. In its electronic ground state, six different conformations have been found (because **AII**, **BII**, and **CII** are identical to **AI**, **BI**, and **CI**, respectively, these three conformations are not considered further). Conformations **AI** and **CI** look the same by inspection of ω_1, ω_2, and ω_3 in Table 1. However, as shown in Figure S2 (Supporting Information), the orientation of the phenol ring in the γ section differs in these two conformers. Contrary to **2H**, all the **2O**$^-$ conformations show almost no deviation from α/β coplanarity, while the amide moiety is completely planar in all conformations. Solvent effects significantly change only the ω_2 torsion for **AI** in ACN: the β and γ sections become perpendicular. The transition to S_1 is accompanied by a single dramatic geometric modification for all **XI*** conformations: the ω_1 angle is −89° (±5° in S_0), and the α and β groups are perpendicular in the excited state. Interestingly, the increase in the polarity of the surroundings allows the recovery of coplanarity for **AI***, **CI***, and **EI*** in benzene, and also for **BI*** in ACN. The **EII*** conformation clearly differs from all other S_1 conformations. The α and β sections remain coplanar, and the γ-section amide bond is characterized by longer C−O bond length (1.275 to 1.294 Å) and sp^3 hybridization of the carbon atom ($\theta \approx 140°$) for all considered environments. As in the case of **2H**, we hypothesize that the latter conformation is related to the chemiluminescence of **2O**$^-$, while other **XI*** conformations are stable fluorescent structures.

The comparison of **2H** and **2O**$^-$ conformations is very instructive. First, the conformation **AI** of **2H** is related to conformations **AI** and **CI** of **2O**$^-$. The same is true for **BI**, **EI** (**2H**), and **EII** (**2O**$^-$). However, there is no structure equivalent to the **2O**$^-$ conformation **BI** for **2H**. Hence, while the modification of the protonation state of **2** does not significantly affect some conformer geometries, other conformations exist in only one protonation state. The most striking difference

Table 3. Natural Bond Orbital Charge Distributions of Conformations EI and EII, EI*, and EII*[a]

				gas phase		in benzene		in ACN	
geometry				S_0	S_1	S_0	S_1	S_0	S_1
2H	EII	α	S_0	0.00	0.00	0.03	0.00	0.04	0.01
			S_1	0.12	0.05	0.20	0.05	0.32	0.06
		β	S_0	0.01	0.01	0.10	0.00	0.10	−0.01
			S_1	−0.08	0.23	−0.16	0.23	−0.21	0.23
		γ	S_0	−0.03	−0.03	−0.16	−0.03	−0.19	−0.03
			S_1	−0.07	−0.29	−0.07	−0.31	−0.14	−0.32
2O$^-$	EI	α	S_0	−0.73		−0.79	−0.81	−0.86	−0.82
			S_1	−0.03		−0.15	−0.05	−0.28	−0.27
		β	S_0	−0.05		−0.01	−0.01	0.03	−0.02
			S_1	−0.69		−0.62	−0.75	−0.54	−0.56
		γ	S_0	−0.23		−0.21	−0.20	−0.20	−0.19
			S_1	−0.23		−0.22	−0.20	−0.20	−0.19
	EII	α	S_0	−0.73	−0.79	−0.80	−0.84	−0.86	−0.89
			S_1	−0.03	−0.23	−0.16	−0.39	−0.28	−0.58
		β	S_0	−0.04	−0.11	−0.01	−0.10	0.03	−0.08
			S_1	−0.70	0.16	−0.63	0.21	−0.54	0.24
		γ	S_0	−0.22	−0.08	−0.21	−0.07	−0.20	−0.04
			S_1	−0.23	−0.90	−0.21	−0.81	−0.20	−0.67

[a]The line entitled geometry indicates the electronic state for which the molecular geometry has been optimized.

between the **2H** and **2O**$^-$ conformations concerns the relative orientation of the α and β sections in S_1: coplanar if **2** is protonated but perpendicular if it is not (as for the *in vacuo* case), while planarity is recovered as a consequence of solvent polarity. The competition between the planar and perpendicular conformations can be related to the topology of S_1 and schematically characterized by the existence of two distinct regions for each conformation. The region close to the Franck−Condon structure corresponds to a planar geometry, while the second region is characterized as perpendicular, with a small energy gap between S_1 and S_0 as evidenced in the following section. The fact that a polar solvent stabilizes the planar structures can be related to the dipole moments of **2H** and **2O**$^-$ in S_1 or to their charge distributions.

Charge Distributions. To highlight the differences in the charge distributions of S_0 and S_1, the NPA charges characterizing the four sections of **2**—α, β, γ, and δ—were computed. Because these data are very similar for conformations **A** to **D**, we report only **AI**(*) and **EI**/**EII**(*) NPA charges in Tables 2 and 3, respectively. The charge distributions obtained for the other conformations are given in the Supporting Information.

The **2H** ground-state charge distributions are roughly the same for all conformations and show a small electronic excess in γ that comes from the central β section (approximately 0.1 |e|). Most often, this distribution is not significantly modified by solvent effects. However, in the case of **EII**, a 0.1 |e| transfer occurs between β and γ when the solvent is present. Preserving the S_0 geometry (vertical excitation), the S_1 charge distribution is significantly different from S_0: a 0.1−0.2 |e| transfer takes place from α (and, to a lesser extent, from γ) to β, while the δ charge remains unaffected by the change in electronic state. This charge transfer is magnified by the presence of the solvent (0.3 |e|). The optimization of each conformer structure in S_1 is accompanied by a modification of these charge distributions. In the gas phase, the **AI*** S_1 charges (+0.13 |e| in β, −0.14 |e| in γ) are very similar to those of S_0 in the ground-state geometry, whereas the conformation **EII*** is characterized by a larger charge separation (+0.23 |e| in β, −0.29 |e| in γ). More interestingly, the **AI*** ground-state charge distribution is not very different from that of S_1, showing only a tiny electron transfer from α to β and γ. A different, more intense electron transfer is observed in **EII***: γ loses 0.26 |e|. Making the same comparison for **AI*** and **EII*** in solvent, a charge transfer greater than 0.2 |e| takes place between β and α in the former, while the latter is characterized by nearly 0.3 |e| flow from γ to β. Hence, in line with the **XI***/**EII*** structural differences highlighted, the vertical $S_1 \rightarrow S_0$ decay is accompanied by different charge transfer mechanisms, depending on whether the emitting state is fluorescent (**XI***) or chemiluminescent (**EII***).

Turning to the **2O**$^-$ conformations **AI**, **EI**, and **EII**, the charge transfer mechanisms are even simpler. In the ground-state geometry, the −1 charge is mainly localized in α as expected (with a non-negligible contribution in γ), and its localization is reinforced by the solvent effect. At the same geometry, the S_1 distribution is completely different; the β section carries a charge between −0.71 |e| (**AI** in gas phase) and −0.54 |e| (**EII** in ACN). Hence, the $S_0 \rightarrow S_1$ transition is characterized by a strong charge transfer between the α and β sections, whatever the conformation. The S_1-optimized structures **AI*** and **EI*** show a charge distribution very similar to the ground state geometry. Conversely, **EII*** exhibits a very large negative charge in γ (from −0.90 |e| in gas phase to −0.67 |e| in ACN), while the α and β charges are negative (from −0.23 |e| in gas phase to −0.58 |e| in ACN) and positive (from 0.16 |e| in gas phase to 0.24 |e| in ACN), respectively. For all conformations, the vertical transition to S_0 is accompanied by a return to the original charge distribution, in which the anion is mostly localized in α. Hence, similar to **2H**, the $S_1 \rightarrow S_0$ charge transfer mechanism (β to α) taking place in (fluorescent) **AI*** and **EI*** anions is different from that of chemiluminescent **EII*** (γ to α and β).

Relative Energies of the Conformers. In the preceeding paragraphs, several conformations of **2H** and **2O**$^-$ in S_0 and S_1 are described. Their energies relative to **AI** or **AI*** are given in Table 4. For **2H** in the gas phase, the **AI** conformation is more stable than those of the other four conformations by at least 2.8 kcal/mol. The presence of solvent reduces the energy gap; all

Table 4. Relative Energies (kcal mol^{-1}) of 2 Conformations

			gas phase	in benzene	in ACN
2H	S_0	**AI**	0.00	0.00	0.00
		BI	3.32	2.12	−0.39
		DI	2.82	1.81	−0.27
		DII	2.79	1.78	−0.38
		EI	3.25	2.03	−0.42
	S_1	**AI***	0.00	0.00	0.00
		BI*	−0.12	2.04	−0.66
		DI*	−0.96	1.48	−0.89
		EII*	3.90	9.12	10.61
2O$^-$	S_0	**AI**	0.00	0.00	0.00
		BI	−3.27	−3.24	−1.75
		CI	−1.11	−1.52	−0.97
		DI	−2.34	−1.86	−0.79
		EI	0.98	0.08	−0.81
		EII	0.74	0.11	−0.81
	S_1	**AI***	0.00	0.00	0.00
		BI*	−1.93	−1.73	−1.68
		CI*	−0.58	−1.18	−0.77
		EI*		1.88	−0.22
		EII*	13.95	13.61	18.25

five conformations are iso-energetic in ACN. In the case of **2O$^-$** in the gas phase, the **BI** conformation is the most stable. Again, the solvent effect reduces the energy differences between the six conformations. Because it was not the aim of this study, we did not further investigate the S_0 potential energy surfaces. It is therefore impossible to determine which conformation would have a lifetime enough long to be detected using UV−vis spectroscopy.

Focusing on the energy differences between minima in S_1, the **EII*** conformation for both protonation states of coelenteramide is clearly destabilized compared to the other **XI*** conformations. For **2H**, **EII*** is 3.90 kcal/mol higher than **AI***, while for **2O$^-$**, **EII*** is 13.95 kcal/mol above **AI***. These energy differences are even larger when solvent effects are added (e.g., 10.61 and 18.25 kcal/mol in ACN). Nevertheless, this excited-state equilibrium structure (**EII***) is accessible along the chemiluminescence reaction from the highly energetic peroxo compound **1**. Together with the structural differences and the contrasting charge distributions highlighted previously, this energy analysis clearly establishes that the **EII*** conformation is indeed chemiluminescent.

Vertical Excitation (Absorption) Energies. The calculated $S_0 \rightarrow S_n$ (n = 1, 2, 3 for **2H**, n = 1, 2, 3, 4 for **2O$^-$**) vertical excitation energies (hereafter denoted T_v) and oscillator strengths f are listed in Table 5 for all ground-state conformations. The experimental spectrum for **2H** in solvents such as DMSO or benzene shows two absorption maxima (298−303 nm and 333−340 nm), separated by approximately 35 nm, that are almost independent of solvent polarity.[23] All conformations give the same T_v values. However, they are approximately 40 nm blue-shifted with respect to the experimental maxima, which is acceptable according to TD-DFT benchmarks.[48,49] For all conformations, the computed $S_0 \rightarrow S_1$ and $S_0 \rightarrow S_2$ excitation energies differ by 13 nm at most, while the S_3 energy is at least 20 nm above S_2. These transitions to three singlet excited states are characterized by large f values, so the first two transitions can be attributed to the experimental lower energy absorption peak, while the third corresponds to the higher energy absorption peak. In the framework of the

Table 5. $S_0 \rightarrow S_n$ Transition Energies T_v (nm) and, in Parentheses, Oscillator Strengths

		gas phase	in benzene	in ACN
2H	**AI**	290 (0.30)	295 (0.58)	292 (0.55)
		280 (0.19)	282 (0.07)	281 (0.07)
		258 (0.26)	262 (0.28)	257 (0.27)
	BI	290 (0.23)	294 (0.58)	289 (0.57)
		282 (0.37)	284 (0.17)	285 (0.12)
		260 (0.20)	262 (0.24)	257 (0.21)
	DI	292 (0.33)	295 (0.60)	296 (0.61)
		283 (0.25)	284 (0.14)	283 (0.10)
		262 (0.24)	262 (0.26)	260 (0.27)
	DII	294 (0.32)	297 (0.56)	297 (0.56)
		281 (0.28)	282 (0.21)	281 (0.18)
		262 (0.22)	263 (0.23)	260 (0.25)
	EI	291 (0.25)	294 (0.52)	290 (0.40)
		279 (0.38)	281 (0.26)	282 (0.30)
		260 (0.19)	261 (0.23)	256 (0.20)
2O$^-$	**AI**	436 (0.20)	407 (0.44)	365 (0.52)
		368 (0.22)	351 (0.65)	317 (0.46)
		366 (0.51)	295 (0.00)	286 (0.01)
		344 (0.00)	286 (0.01)	277 (0.09)
	BI	432 (0.27)	406 (0.58)	366 (0.63)
		372 (0.56)	352 (0.60)	320 (0.45)
		359 (0.01)	292 (0.00)	280 (0.03)
		353 (0.18)	284 (0.00)	279 (0.08)
	CI	434 (0.21)	406 (0.45)	365 (0.52)
		379 (0.18)	351 (0.64)	318 (0.48)
		368 (0.03)	292 (0.01)	283 (0.01)
		360 (0.50)	286 (0.01)	277 (0.09)
	DI	434 (0.27)	407 (0.56)	366 (0.62)
		368 (0.75)	352 (0.62)	319 (0.44)
		349 (0.02)	292 (0.01)	280 (0.05)
		335 (0.00)	285 (0.00)	279 (0.06)
	EI	420 (0.22)	398 (0.56)	364 (0.61)
		367 (0.01)	349 (0.60)	319 (0.44)
		363 (0.22)	290 (0.00)	283 (0.01)
		356 (0.54)	286 (0.00)	277 (0.09)
	EII	419 (0.23)	399 (0.58)	364 (0.61)
		368 (0.49)	352 (0.58)	319 (0.44)
		365 (0.23)	290 (0.00)	283 (0.01)
		349 (0.08)	286 (0.00)	277 (0.09)

TD-DFT method, these three excited states are mainly characterized by electron density flowing from the 4-hydroxyphenyl (α) to the pyrazine (β) section (transition densities are depicted in Figure 3), as confirmed by inspection of charge distributions in Table 2. However, in looking more precisely at which orbitals are primarily involved in the excitation and in comparing the oscillator strengths, it is clear that the order between S_1 and S_2 depends on the conformation. The increasing polarity of the solvent does not significantly modify T_v values. However, while the $S_0 \rightarrow S_3$ f values remain unchanged, one of the two other transitions becomes more intense, and the other one becomes less intense. Moreover, the ordering between S_1 and S_2 can differ from that found in the gas phase, such as in the case of conformation **BI**.

For anionic **2O$^-$**, in contrast to **2H**, the first excited state can easily be distinguished because it is separated from the other states by more than 50 nm. Given the corresponding transition density in Figure 3, S_1 can be described as a transition from α to β. The next three excited states, S_2 to S_4, appear in a small

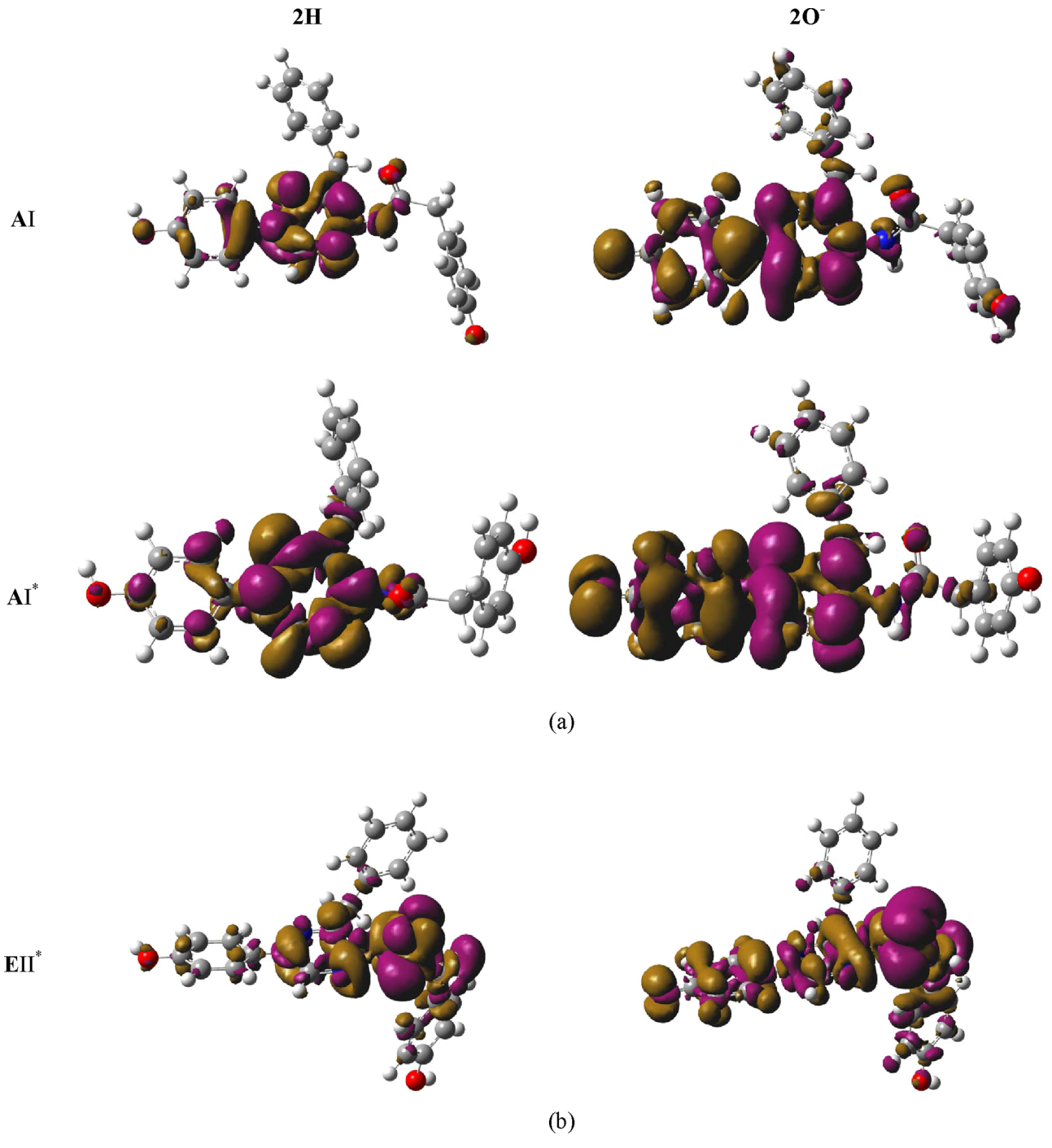

Figure 3. Electronic density differences between S_0 and S_1 for (a) **AI** and **AI*** conformations and (b) **EII*** conformation.

energetic window (10 nm large for **EI** to 30 nm for **DI**), and their ordering depends on the conformation. In all cases, one state is very bright ($f > 0.49$), another is completely dark ($f \approx 0.00$), and the last is intermediate ($f \approx 0.20$), with the exception of conformation **DI** (dark state). The solvent effect is very interesting; it stabilizes the first excited state by more than 50 nm (from the gas phase to ACN), and the absorption toward S_1 is enhanced (f increases by a factor 2 or more). All other excited states are affected by solvent. One state remains very bright, while the other transitions are less efficient ($f < 0.1$). This last result is in perfect agreement with experiments, which show two absorption peaks at 328 and 380 nm for $\mathbf{2O^-}$ in benzene.[23] Note that TD-DFT T_v values differ by only 20 to 30 nm.

The small solvent effect in the **2H** excitation energies and the large effect in $\mathbf{2O^-}$ can be related to the very different $S_0 \rightarrow S_1$ charge redistribution mentioned above (Tables 2 and 3). It can be deduced from the NPA charges that the S_1 dipole moment for every **2H** conformation is always smaller than that of $\mathbf{2O^-}$. Consequently, $\mathbf{2O^-}$ excited states are more stabilized by solvent than is **2H**.

Surrounding effects are not always isotropic. We investigated the influence of a simple base (NH_3) close to the phenol proton in the α section. Because the conformational effect on the absorption spectra is small, the most stable conformer **AI** in

S_0 for the **2H** species is selected to build a **2H** + NH_3 complex in the implicit benzene solvent, allowing direct comparison with experimental results for the **2** ion pair.[23] The TD-DFT-predicted vertical transitions to S_1 are summarized in Table 6.

Table 6. Modifications of the Transition Energies T_v, T_e (nm, Oscillator Strengths f in Parentheses) of 2H + NH_3 in Benzene, Along the Increasing Bond Length R(O−H) (Å)

	AI	AI*	EII*
R(O−H)	T_v (f)	T_e (f)	T_e (f)
optimized	300 (0.59)	364 (0.71)	526 (0.00)
1.200	313 (0.62)	373 (0.66)	542 (0.00)
1.400	328 (0.61)	387 (0.58)	567 (0.00)
1.600	339 (0.59)	397 (0.52)	589 (0.00)
1.800	347 (0.58)	406 (0.47)	608 (0.00)
2.000	354 (0.58)	413 (0.44)	623 (0.00)
2.200	359 (0.57)	419 (0.41)	637 (0.00)
2.400	363 (0.56)	424 (0.39)	649 (0.00)
2.600	367 (0.56)	429 (0.37)	659 (0.00)
2.800	370 (0.56)	434 (0.36)	670 (0.00)
3.000	373 (0.55)	438 (0.34)	678 (0.00)
4.000	382 (0.52)		708 (0.00)

When the O_{13}−H_{14} bond length increases, the **2H** geometry evolves toward $\mathbf{2O^-}$. The T_v value gradually increases along this transformation, while the oscillator strength increases (f = 0.59 → 0.62) and then decreases to f = 0.52. Hence, the less covalent the O_{13}−H_{14} bond, the larger the vertical excitation energy. This relationship is clear if we assume that α is a much stronger acid in S_1 than in S_0. Hence, **2H** in the ground state forms a weaker H-bonded complex with NH_3 (equilibrium N−H_{14} distance is 1.76 Å in benzene, 1.70 Å in ACN) than in the excited state (1.68 Å in benzene, 1.59 Å in ACN). This trend is in good agreement with the experimental results.[11−14] Given the TD-DFT absorption error of 40 nm, a tiny elongation of the bond is enough to reproduce the experimental 337 nm excitation maximum of **2** in benzene + *n*-butylamine.[23] Our results confirm that the absorption properties of **2H** can be modulated by the covalent character of the O_{13}−H_{14} bond.[11,12]

Vertical Emission (Fluorescence and Chemiluminescence) Energies. The computed vertical emission energies (hereafter denoted T_e) and f values for the lowest-lying singlet excited states of all conformations (4 for **2H**, 5 for $\mathbf{2O^-}$) are reported in Table 7. In the fluorescence experiment, the emission spectrum was recorded by excitation at the wavelength of the absorption maximum, which means that only one emission peak was measured (387 nm for **2H** in benzene, 399 nm for **2H** in ACN, 485−522 nm for $\mathbf{2O^-}$ in benzene).[23] In the gas phase, the fluorescent **2H** conformation **AI*** exhibits T_e values that are very different from those of **BI*** and **DI***. In the former conformation, the S_1 state is much less fluorescent (375 nm, f = 0.11). Because S_0→S_1 and S_0→S_3 transitions in **AI** show comparable efficiency (Table 5), it cannot be ruled out that **AI** fluorescence also involves a complex, nonradiative pathway starting at S_3. In the **BI*** and **DI*** conformations, S_1 is a bright fluorescent state (341 nm, f = 0.56). When the implicit solvent is added to models, all three conformations show the same photophysical properties, including very efficient emission from S_1 (353 to 371 nm and f = 0.73 to 1.01 in benzene, 354 to 380 nm and f = 0.79 to 1.02 in ACN). Comparison to experiment shows that TD-DFT results must be corrected by a 20-nm blue-shift. Nevertheless, the 10-nm benzene-to-ACN solvent shift is correctly reproduced.

Table 7. S_1→S_0 Transition Energies T_e (nm) with Oscillator Strengths in Parentheses

		gas phase	in benzene	in ACN
2H	**AI***	375 (0.11)	360 (0.73)	380 (0.94)
	BI*	341 (0.55)	371 (1.01)	354 (0.79)
	DI*	341 (0.56)	353 (0.80)	371 (1.02)
	EII*	524 (0.00)	515 (0.00)	509 (0.00)
$\mathbf{2O^-}$	**AI***	824 (0.00)	498 (0.20)	443 (0.72)
	BI*	783 (0.00)	577 (0.00)	443 (0.84)
	CI*	811 (0.00)	495 (0.20)	443 (0.72)
	EI*		439 (0.82)	482 (0.24)
	EII*	1333 (0.00)	849 (0.00)	612 (0.00)

In the gas phase, $\mathbf{2O^-}$ conformations in S_1 are characterized by an α ring almost perpendicular to β. Accordingly, all S_1→S_0 oscillator strengths are near zero: $\mathbf{2O^-}$ does not emit light in vacuo. Note that the calculated T_e values are quite small and lie outside the range of visible light. However, as can be expected from the different charge distributions in S_0 and S_1, the solvent can strongly modify gas phase emission properties. Indeed, **AI***, **CI***, and **EI*** are fluorescent in benzene, while all four conformations can emit light in ACN. This can be related to a return to the α/β coplanar orientation. While the S_1→S_0 transitions for **AI*** and **CI*** in benzene are less intense than for **EI***, in ACN, emission becomes very efficient (f = 0.72 to 0.84) for **AI***, **BI***, and **CI***, but it does not change for **EI***. This result demonstrates the multiconformational origin of the fluorescence of $\mathbf{2O^-}$ and may explain the observed broadening of its emission spectrum.[23]

There are few experimental data on chemiluminescence of **2H** or $\mathbf{2O^-}$ (or analogues) in the gas phase or solvent.[14,22] Our calculations suggest that the only conformation that can be associated with the chemiluminescence reaction, **EII***, is completely dark for all protonation states and in all surroundings. This result may explain why none of the computed vertical emission energies matched the experimental estimate (approximately 465 nm[14,22]). Actually, the S_1→S_0 gap for $\mathbf{2O^-}$ in the gas phase is very small (1333 nm). The solvent effect modifies the emission energy dramatically: 849 and 612 nm in benzene and ACN, respectively. This solvent effect is a direct consequence of the large charge separation in the chemiluminescent state, as has already been shown. In fact, the main orbital excitations involved in this electronic transition are localized to sections of the molecule that are nearly orthogonal (see Table S4, Supporting Information). Accordingly, the overlap between these π orbitals nearly vanishes. Hence, whatever the energy gap (modified by the solvent), the oscillator strength remains close to 0.

Finally, it is interesting to determine whether the presence of a base can affect the emission (fluorescence and chemiluminescence) properties of **2**, as is the case for absorption (Table 6). Both the fluorescence from **AI*** and chemiluminescence from **EII*** are red-shifted when the O_{13}−H_{14} bond is weakened and fluorescence efficiency is significantly reduced, while the chemiluminescent state remains dark.

Discussion: Possible Chemiluminescence Mechanisms. The most striking result of this study concerns the computed darkness of the chemiluminescent state. Recall that the fluorescence and bioluminescence properties of Ca^{2+}-discharged photoproteins (obelin and clytin) are different.[17,50]

Moreover, the coelenterazine chemiluminescence emission maximum is the same as the bioluminescence emission maximum, but its fluorescence emission maximum is red-shifted by nearly 50 nm.[22] Teranishi and Goto studied the chemiluminescence of coelenterazine analogues in dimethyl sulfoxide.[51,52] They found that an electron-donating group in the *para* position to the α section (replacing the OH group) does not increase chemiluminescence efficiency, implying that the electron density localized on the phenyl group is not directly involved in the chemiluminescence mechanism.

Direct comparison of our results to experimental data is not straightforward. The protonation state of the coelenteramide may differ between the gas phase, solvent, or protein environments. In this work, we consider only the neutral amide (γ section) as the most probable light emitter involved in the bioluminescence mechanism. While the absorption and fluorescence properties of **2** compare well with coelenteramide and analog experimental data,[23] we found that the chemiluminescent state is dark. This apparent contradiction can be explained with several hypotheses:

1. TD-DFT results, using the CAM-B3LYP functional together with the 6-31+G(d,p) basis set, cannot describe the chemiluminescent state. This possibility seems unlikely because the geometries and charge distributions obtained for **EII*** are very similar to those obtained for the model molecule, whose properties have been computed at the reliable *ab initio* CASPT2 level of theory.[26]
2. Neither **2H** nor $\mathbf{2O^-}$ are chemiluminescent species in the gas phase or in the solvents considered in this study. While the very small $S_1 \rightarrow S_0$ energy gap for $\mathbf{2O^-}$ in the gas phase may suggest nonradiative decay to the ground state in the vicinity of the **EII*** geometry, the other energy differences (T_e < 850 nm) exclude this possibility.
3. Chemiluminescence light emission takes place in another region of the S_1 potential energy surface that corresponds to an electronic structure different from that found for **EII***. In fact, this geometry is not significantly different from the chemiluminescence reaction TS, and it lies at an energy much higher than any other computed S_1 minimum. Hence, it can be hypothesized that this stored energy is large enough to overcome the S_1 energy barrier(s), as in Figure 4. Note that if one of the next minimum-energy structures can emit light, it may or may not coincide with one of the fluorescent minima **XI*** found in this work. If this is the case, the luminescent and fluorescent states would be the same. If it is not the case, the evolution of the system will be governed by competition between emission efficiency from this local minimum and the motion in S_1 toward the most stable minima. The proposed mechanism implies that a region of near-degeneracy between the chemiluminescent state and a fluorescent state stands in the vicinity of the barrier. To test this hypothesis, a simple 1D investigation of the S_1 potential energy surface, starting from the **EII*** structure, was performed along each of the relevant degrees of freedom, namely R and θ. As shown in Table 8, both degrees of freedom are largely independent and the S_1 energy continuously increases, except in the case of θ for **2H**, which shows a local maximum around θ = 170°. While the energy gap between the chemiluminescent state and the ground state increases, the same quantity calculated from the closest fluorescent state (S_2) is not affected by these local structural modifications. This result was expected because the fluorescent state is characterized by an electronic density difference that is essentially localized to the α and β moieties, whereas chemiluminescence extends into the γ section (Figure 3). Accordingly, the energy gap between the chemiluminescent and fluorescent states decreases from 1.6 eV to less than 0.8 eV when the amide moiety becomes planar. The calculations used here are too crude to allow a definitive answer, but they definitively support the proposed mechanism.

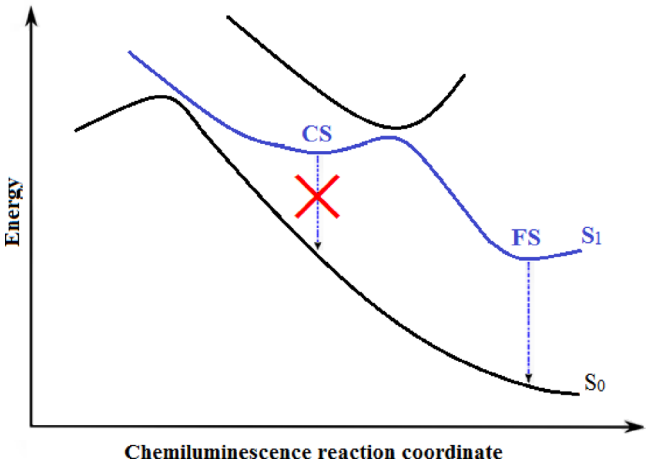

Figure 4. Schematic representation of the electronic sates involved in the chemiluminescence process. CS stands for the chemiluminescent state, while FS stands for fluorescent state.

Table 8. 1D Relaxed Scan of R (Å) and θ (deg) Degrees of Freedom, Starting from EII* Structures[a]

	θ	$R(C_8-O_9)$	S_1 energy	T_e (CS)/S_1	T_e (FS) /$S_{2/3}$
2H	139	1.286	0.00	2.36	3.98
	149	1.287	0.61	2.68	4.00
	159	1.290	1.89	2.92	4.02
	169	1.292	2.95	3.07	4.03
	179	1.291	2.67	3.16	4.00
$\mathbf{2O^-}$	138	1.275	0.00	0.93	2.60
	148	1.274	0.74	1.27	2.56
	158	1.273	2.31	1.56	2.57
	168	1.272	4.01	1.77	2.59
	178	1.274	5.34	1.87	2.60
2H	139	1.286	0.00	2.36	3.98
	139	1.276	0.05	2.41	3.98
	139	1.266	0.22	2.45	3.97
	139	1.256	0.52	2.49	3.96
	139	1.246	0.93	2.53	3.96
	138	1.236	1.48	2.57	3.95
	138	1.226	2.17	2.60	3.94
	138	1.216	3.01	2.62	3.93
$\mathbf{2O^-}$	138	1.275	0.00	0.93	2.55
	138	1.265	0.06	0.97	2.55
	139	1.255	0.26	1.01	2.55
	139	1.245	0.59	1.05	2.55
	139	1.235	1.08	1.09	2.55
	139	1.225	1.72	1.12	2.55

[a] S_1 relative energies in kcal mol^{-1}, T_e in eV.

dx.doi.org/10.1021/ct300356j | J. Chem. Theory Comput. 2012, 8, 2796−2807

Based on the present findings, we are primarily concerned with the bioluminescence process. If we assume that **2H** and $\mathbf{2O}^-$ are not chemiluminescent in their respective **E**II* conformations, proteins may be responsible for their bioluminescence, for example, by modifying the S_1 potential energy surface topology involved in the reaction path or modifying the electronic structure in such a way that the decay probability increases. In that case, the protein would act as a switch capable of initiating coelenterazine (bio)luminescence at a wavelength different from its fluorescence (obelin and clytin)[17,50] or similar to it (aequorin).[53,54]

CONCLUSION

The fluorescence spectra of coelenteramide and the chemiluminescence of coelenterazine were theoretically investigated at the TD-DFT level of theory in the gas phase and in implicit models for benzene and ACN solvents. A systematic exploration of the conformational space for neutral and phenolate anion species was performed. The computed vertical transitions (absorption and emission) agree well with the available experimental results. The fluorescent state was characterized by a rather localized charge transfer from 4-hydroxyphenyl to the pyrazine moiety, while the chemiluminescent state was characterized by a long-range charge transfer from the amide group to the 4-hydroxyphenyl moiety. The spectroscopic properties of **2** are modulated by the polarity of its environment and also by the covalent character of the O−H bond in the 4-hydroxyphenyl section.

The computed darkness of the chemiluminescent structure is the most surprising result. This apparent contradiction can be overcome if we make the following hypothesis: while the first minimum in the excited state of the chemiluminescence process is nonemitting, the reacting molecule stores enough energy to overcome a barrier and reach a light-emitting minimum. The validation of such a hypothesis will benefit from further experimental and theoretical investigation into coelenterazine chemiluminescence dynamical properties.

This study constitutes another step in the theoretical investigation of coelenterazine luminescence and raises new questions that will be addressed soon.

ASSOCIATED CONTENT

Supporting Information

Natural bond orbital charges of the B, C, and D conformations. Key degrees of freedom characterizing the computed transition state structures. Geometric parameters for the CS structure. Comparison of CASPT2 and TD-DFT transition energies. Superposition of various coelenteramide conformations. Cartesian coordinates for all coelenteramide conformations. This information is available free of charge via the Internet at http://pubs.acs.org.

AUTHOR INFORMATION

Corresponding Author

*E-mail: nicolas.ferre@univ-amu.fr (N.F.); yajun.liu@bnu.edu.cn (Y.-J.L.).

Notes

The authors declare no competing financial interest.

ACKNOWLEDGMENTS

N.F. thanks Dr. M. Huix-Rotllant for fruitful discussions about TD-DFT. S.-F.C., N.F., and Y.-J.L. thank the Chinese−French PHC Cai Yuanpei program for funding (Project No. 23982SE). I.N. thanks Prof. H. M. Marques for funding through the DST/NRF SARChI initiative. D.R.-S. thanks the European Research Council under the European Community's Seventh Framework Program (FP7/2007-2013)/ERC Grant Agreements No. 255363. R.L. thanks the Swedish Research Council (VR) for financial support. Some calculations were performed at the Centre Régional de Compétences en Modélisation Moléculaire in Marseille, France.

REFERENCES

(1) Thomson, C. M.; Herring, P. J.; Campbell, A. K. *J. Biolumin. Chemilumin.* **1997**, *12*, 87−91.
(2) Rees, J. F.; Thompson, E. M.; Baguet, F.; Tsuji, F. I. *Comp. Biochem. Physiol., Part A: Mol. Integr. Physiol.* **1990**, *96*, 425−430.
(3) Campbell, A. K.; Herring, P. J. *Mar. Biol. (Heidelberg, Ger.)* **1990**, *104*, 219−225.
(4) Shimomura, O.; Inoue, S.; Johnson, F. H.; Haneda, Y. *Comp. Biochem. Physiol., Part B: Biochem. Mol. Biol.* **1980**, *65*, 435−437.
(5) McCapra, F.; Hart, R. *Nature* **1980**, *286*, 660−661.
(6) Shimomura, O. *Bioluminescence: Chemical Principles and Methods*; World Scientific Publishing: Singapore, 2006; pp 91−185.
(7) Cormier, M. J.; Hori, K.; Karkhanis, Y. D.; Anderson, J. M.; Wampler, J. E.; Morin, J. G.; Hastings, J. W. *J. Cell. Physiol.* **1973**, *81*, 291−297.
(8) Shimomura, O.; Johnson, F. H. *Biochemistry* **1972**, *11*, 1602−1608.
(9) Vysotski, E. S.; Lee, J. *Acc. Chem. Res.* **2004**, *37*, 405−415.
(10) Navizet, I.; Liu, Y. J.; Ferré, N.; Roca-Sanjuán, D.; Lindh, R. *ChemPhysChem* **2011**, *12*, 3064−3076.
(11) Mori, K.; Maki, S.; Niwa, H.; Ikeda, H.; Hirano, T. *Tetrahedron* **2006**, *62*, 6272−6288.
(12) Imai, Y.; Shibata, T.; Maki, S.; Niwa, H.; Ohashi, M.; Hirano, T. *J. Photochem. Photobiol., A* **2001**, *146*, 95−107.
(13) Saito, R.; Hirano, T.; Niwa, H.; Ohashi, M. *J. Chem. Soc., Perkin Trans. 2* **1997**, 1711−1716.
(14) Hirano, T.; Mizoguchi, I.; Yamaguchi, M.; Chen, F. Q.; Ohashi, M.; Ohmiya, Y.; Tsuji, F. I. *J. Chem. Soc., Chem. Commun.* **1994**, *2*, 165−167.
(15) Deng, L.; Markova, S. V.; Vysotski, E. S.; Liu, Z. J.; Lee, J.; Rose, J.; Wang, B. C. *J. Biol. Chem.* **2004**, *279*, 33647−33652.
(16) Liu, Z. J.; Stepanyuk, G. A.; Vysotski, E. S.; Lee, J.; Markova, S. V.; Malikova, N. P.; Wang, B. C. *Proc. Natl. Acad. Sci. U.S.A.* **2006**, *103*, 2570−2575.
(17) Markova, S. V.; Vysotski, E. S.; John, R.; Burakova, L. P.; Wang, B. C.; Lee, J. *Biochemistry* **2002**, *41*, 2227−2236.
(18) Stepanyuk, G. A.; Golz, S.; Markova, S. V.; Frank, L. A.; Lee, J.; Vysotski, E. S. *FEBS Lett.* **2005**, *579*, 1008−1014.
(19) van Oort, B.; Eremeeva, E. V.; Koehorst, R. B. M.; Laptenok, S. P.; van Amerongen, H.; van Berkel, W. J. H.; Malikova, N. P.; Markova, S. V.; Vysotski, E. S.; Visser, A. J. W. G.; Lee, J. *Biochemistry* **2009**, *48*, 10486−10491.
(20) Belogurova, N. V.; Kudryasheva, N. S.; Alieva, R. R.; Sizykh, A. G. *J. Photochem. Photobiol., B* **2008**, *92*, 117−122.
(21) Malikova, N. P.; Stepanyuk, G. A.; Frank, L. A.; Markova, S. V.; Vysotski, E. S.; Lee, J. *FEBS Lett.* **2003**, *554*, 184−188.
(22) Wu, C.; Nakamura, H.; Murai, A.; Shimomura, O. *Tetrahedron Lett.* **2001**, *42*, 2997−3000.
(23) Shimomura, O.; Teranishi, K. *Luminescence* **2000**, *15*, 51−58.
(24) Isobe, H.; Yamanaka, S.; Okumura, M.; Yamaguchi, K. *J. Phys. Chem. A* **2009**, *113*, 15171−15187.
(25) Tomilin, F. N.; Antipina, L. Y.; Vysotski, E. S.; Ovchinnikov, S. G.; Gitelzon, I. I. *Dokl. Biochem. Biophys.* **2008**, *422*, 279−284.
(26) Roca-Sanjuán, D.; Delcey, M.; Navizet, I.; Ferré, N.; Liu, Y. J.; Lindh, R. *J. Chem. Theory Comput.* **2011**, *7*, 4060−4069.
(27) Perdew, J.; Ruzsinszky, A.; Tao, J.; Staroverov, V.; Scuseria, G.; Csonka, G. *J. Chem. Phys.* **2005**, *123*, 062201.

(28) Dreuw, A.; Head-Gordon, M. *Chem. Rev.* **2005**, *105*, 4009−4037.
(29) Stratmann, R.; Scuseria, G.; Frisch, M. *J. Chem. Phys.* **1998**, *109*, 8218.
(30) Runge, E.; Gross, E. *Phys. Rev. Lett.* **1984**, *52*, 997−1000.
(31) Peach, M.; Helgaker, T.; Sa ek, P.; Keal, T.; Lutn s, O.; Tozer, D.; Handy, N. *Phys. Chem. Chem. Phys.* **2006**, *8*, 558−562.
(32) Yanai, T.; Tew, D.; Handy, N. *Chem. Phys. Lett.* **2004**, *393*, 51−57.
(33) Liu, F.; Liu, Y.; De Vico, L.; Lindh, R. *J. Am. Chem. Soc.* **2009**, *131*, 6181−6188.
(34) Chung, L. W.; Hayashi, S.; Lundberg, M.; Nakatsu, T.; Kato, H.; Morokuma, K. *J. Am. Chem. Soc.* **2008**, *130*, 12880−12881.
(35) Liu, F.; Liu, Y.; Vico, L. D.; Lindh, R. *Chem. Phys. Lett.* **2009**, *484*, 69−75.
(36) Cossi, M.; Rega, N.; Scalmani, G.; Barone, V. *J. Chem. Phys.* **2001**, *114*, 5691.
(37) Barone, V.; Cossi, M. *J. Phys. Chem. A* **1998**, *102*, 1995−2001.
(38) Cossi, M.; Rega, N.; Scalmani, G.; Barone, V. *J. Comput. Chem.* **2003**, *24*, 669−681.
(39) Reed, A. E.; Weinstock, R. B.; Weinhold, F. *J. Chem. Phys.* **1985**, *83*, 735.
(40) Frisch, M.; Trucks, G.; Schlegel, H.; Scuseria, G.; Robb, M.; Cheeseman, J.; Scalmani, G.; Barone, V.; Mennucci, B.; Petersson, G.; Nakatsuji, H.; Caricato, M.; Li, X.; Hratchian, H. P.; Izmaylov, A. F.; Bloino, J.; Zheng, G.; Sonnenberg, J. L.; Hada, M.; Ehara, M.; Toyota, K.; Fukuda, R.; Hasegawa, J.; Ishida, M.; Nakajima, T.; Honda, Y.; Kitao, O.; Nakai, H.; Vreven, T.; Montgomery, J. A., Jr.; Peralta, J. E.; Ogliaro, F.; Bearpark, M.; Heyd, J. J.; Brothers, E.; Kudin, K. N.; Staroverov, V. N.; Kobayashi, R.; Normand, J.; Raghavachari, K.; Rendell, A.; Burant, J. C.; Iyengar, S. S.; Tomasi, J.; Cossi, M.; Rega, N.; Millam, J. M.; Klene, M.; Knox, J. E.; Cross, J. B.; Bakken, V.; Adamo, C.; Jaramillo, J.; Gomperts, R.; Stratmann, R. E.; Yazyev, O.; Austin, A. J.; Cammi, R.; Pomelli, C.; Ochterski, J. W.; Martin, R. L.; Morokuma, K.; Zakrzewski, V. G.; Voth, G. A.; Salvador, P.; Dannenberg, J. J.; Dapprich, S.; Daniels, A. D.; Farkas, A.; Foresman, J. B.; Ortiz, J. V.; Cioslowski, J.; Fox, D. J. *Gaussian 09*, Revision A.02; Gaussian, Inc.: Wallingford, CT, 2009.
(41) Kirkpatrick, S.; Gelatt, C. D.; Vecchi, M. P. *Science* **1983**, *220*, 671−680.
(42) Stewart, J. J. P. *J. Mol. Model.* **2007**, *13*, 1173−1213.
(43) Hu, C.; Hirai, H.; Sugino, O. *J. Chem. Phys.* **2007**, *127*, 064103.
(44) Levine, B. G.; Ko, C.; Quenneville, J.; Martínez, T. J. *Mol. Phys.* **2006**, *104*, 1039−1051.
(45) Tapavicza, E.; Tavernelli, I.; Rothlisberger, U.; Filippi, C.; Casida, M. E. *J. Chem. Phys.* **2008**, *129*, 124108.
(46) Minezawa, N.; Gordon, M. S. *J. Phys. Chem. A* **2009**, *113*, 12749−12753.
(47) Hirano, T.; Ohmiya, Y.; Maki, S.; Niwa, H.; Ohashi, M. *Tetrahedron Lett.* **1998**, *39*, 5541−5544.
(48) Jacquemin, D.; Wathelet, V.; Perpète, E. A.; Adamo, C. *J. Chem. Theory Comput.* **2009**, *5*, 2420−2435.
(49) Perpète, E. A.; Jacquemin, D. *J. Mol. Struct.: THEOCHEM* **2009**, *914*, 100−105.
(50) Markova, S. V.; Burakova, L. P.; Frank, L. A.; Golz, S.; Korostileva, K. A.; Vysotski, E. S. *Photochem. Photobiol. Sci.* **2010**, *9*, 757−765.
(51) Teranishi, K.; Goto, T. *Chem. Lett.* **1989**, *18*, 1423−1426.
(52) Teranishi, K.; Goto, T. *Bull. Chem. Soc. Jpn.* **1990**, *63*, 3132−3140.
(53) Shimomura, O. *Biochem. J.* **1995**, *306*, 537−543.
(54) Shimomura, O.; Johnson, F. H. *Nature* **1970**, *227*, 1356−1357.